

# Hydro-thermo-mechanical biaxial buckling analysis of sandwich micro-plate with isotropic/orthotropic cores and piezoelectric/polymeric nanocomposite face sheets based on FSDT on elastic foundations

Javad Rajabi and Mehdi Mohammadimehr\*

Department of Solid Mechanics, Faculty of Mechanical Engineering, University of Kashan, P.O. Box: 87317-53153, Kashan, Iran

(Received May 30, 2019, Revised August 5, 2019, Accepted October 14, 2019)

**Abstract.** In the present work, the buckling analysis of micro sandwich plate with an isotropic/orthotropic cores and piezoelectric/polymeric nanocomposite face sheets is studied. In this research, two cases for core of micro sandwich plate is considered that involve five isotropic Devineycell materials (H30, H45, H60, H100 and H200) and an orthotropic material also two cases for facesheets of micro sandwich plate is illustrated that include piezoelectric layers reinforced by carbon and boron-nitride nanotubes and polymeric matrix reinforced by carbon nanotubes under temperature-dependent and hydro material properties on the elastic foundations. The first order shear deformation theory (FSDT) is adopted to model micro sandwich plate and to apply size dependent effects from modified strain gradient theory. The governing equations are derived using the minimum total potential energy principle and then solved by analytical method. Also, the effects of different parameters such as size dependent, side ratio, volume fraction, various material properties for cores and facesheets and temperature and humidity changes on the dimensionless critical buckling load are investigated. It is shown from the results that the dimensionless critical buckling load for boron nitride nanotube is lower than that of for carbon nanotube. It is illustrated that the dimensionless critical buckling load for Devineycell H200 is highest and lowest for H30. Also, the obtained results for micro sandwich plate with piezoelectric facesheets reinforced by carbon nanotubes (case b) is higher than other states (cases a and c). The results of this research can be used in aircraft, automotive, shipbuilding industries and biomedicine.

**Keywords:** biaxial buckling analysis; micro sandwich plate; isotropic and orthotropic cores; piezoelectric layers reinforced by carbon and boron nitride nanotubes facesheets; polymeric matrix reinforced by carbon nanotubes; temperature-dependent and hydro material properties; micro-mechanical and the extended rule of mixture approaches

## 1. Introduction

Due to high stiffness and relatively light weight, micro sandwich structures such as beams, plates, and shells are extensively employed across wide range of engineering applications including aerospace, automotive, construction and biomedical industries (Vinson 2005, Ghorbanpour Arani *et al.* 2011, Zhang *et al.* 2015, 2019, Mohammadimehr *et al.* 2016a, b, c, Mohammadimehr and Alimirzaei 2017, Mohammadimehr and Mehrabi 2017, Birman and Kardomateas 2018, Sofiyev 2018, Kim *et al.* 2019, Bahaadini and Saidi 2019, Arshid *et al.* 2019, Ghorbanpour Arani and Soleymani 2019). Thus, employing stiff facesheets such as carbon nanotubes (CNT) reinforced composite and low specific weight core is suggested. Some researchers investigated the bending, buckling and vibration analysis of sandwich micro beams, plates and shells that illustrated as follows:

Ghorbanpour Arani *et al.* (2012) presented the obtained stress analysis of a long piezoelectric polymeric hollow

cylinder reinforced with carbon nanotube (CNT) under magneto-thermo-electro-mechanical loadings. They used the rule of mixture and modified multiscale bridging model to predict effective properties of nanocomposite and concluded that increasing CNT volume fraction enhances strength of the nanocomposite cylinder. In the other work, Mohammadimehr *et al.* (2015) investigated free vibration of viscoelastic double-bonded polymeric nanocomposite plates reinforced by FG-SWCNTs using MSGT, sinusoidal shear deformation theory and meshless method. Sofiyev (2014) considered the vibration and buckling analysis of sandwich cylindrical shells covered by different types of coatings such as functionally graded (FG), metal and ceramic coatings subjected to a uniform hydrostatic pressure using first order shear deformation theory (FSDT). Mohammadimehr *et al.* (2016e) illustrated electro-elastic analysis of a sandwich thick plate considering FG core and composite piezoelectric layers on Pasternak foundation using TSDT. Sofiyev *et al.* (2016) investigated the effects of shear stresses and rotary inertia on the stability and vibration of sandwich cylindrical shells with FGM core surrounded by elastic medium (resting on Pasternak foundation) based on FSDT. Mohammadimehr and Shahedi (2017) demonstrated high-order buckling and free

\*Corresponding author, Associate Professor,  
E-mail: mmohammadimehr@kashanu.ac.ir

vibration analysis of two types sandwich beam including AL or PVC-foam flexible core and CNTs reinforced nanocomposite face sheets using GDQM. Yang and He (2017) considered the buckling analysis of an orthotropic functionally graded (FG) micro-plate on the basis of a re-modified couple stress theory. They investigated simultaneously the macro- and microscopic anisotropy by introducing two material length scale parameters. Sofiyev *et al.* (2017) studied the dynamic instability of FG orthotropic conical shells using various shear deformation shell theories (SDT) such as FSDT and higher order shear deformation theory (HSDT) that the conical shell is made from functionally graded (FG) orthotropic material. They employed in their formulation of problem a dynamic version of Donnell's shell theory and then converted the equations to a Mathieu-Hill type differential equation by employing Galerkin's method. Also, they found the boundaries of main instability zones by applying the method proposed by Bolotin. Hajmohammad *et al.* (2018) presented bending and buckling analyses of functionally graded material (FGM) annular sandwich microplate integrated with piezoelectric layers subjected to radial compressive and uniform transverse load. They considered layerwise theory in their equations. Mohammadimehr and Mehrabi (2018) illustrated vibration and stability analyses of double-bonded micro composite sandwich piezoelectric tubes conveying fluid flow under electro-thermo-mechanical loadings. They obtained the governing equations of motion based on Hamilton's principle and solved by differential quadrature method (DQM). Ansari *et al.* (2018) presented a comprehensive numerical study on the large-amplitude free vibration of sandwich annular plates integrated with functionally graded carbon nanotube-reinforced composite (FG-CNTRC) face sheets resting on elastic foundation. They considered the sandwich plate made of a homogeneous core and two FG-CNTRC face sheets whose material properties are estimated through a micromechanical model. Since the fundamental vibrational mode shapes of annular plates are axisymmetric, they derived the governing equations assuming the axisymmetric formulation. Sobhy and Zenkour (2018) investigated the effect of the magnetic field on the thermo-mechanical buckling and vibration of viscoelastic sandwich nanobeams in humid environment. They took into account the nanoscale beam composed of a homogeneous core integrated with two FG carbon nanotube (CNT) reinforced face sheets. Moradi-Dastjerdi and Aghadavoudi (2018) obtained the stress distribution and deflection in sandwich plates with FG nanocomposite face sheets by a first order shear deformation theory (FSDT) based mesh-free method. Li *et al.* (2018) presented the nonlinear vibration and the dynamic buckling of a graphene platelet reinforced sandwich functionally graded porous (GPL-SFGP) plate that considered the GPL-SFGP plate consists of two metal face layers and a functionally graded porous core with graphene platelet reinforcement and the open-cell metal foam model to model the mechanical properties of the porous core. Liu *et al.* (2019) aroused usually porosity of functionally graded materials (FGMs) by fabrication defects. They proved that the porosity has a significant

influence on the static responses of their structures, but the effects of porosity on buckling behaviors are still worth investigating. To reveal these effects, they investigated the thermal-mechanical coupling buckling issue of a clamped-clamped porous FGM sandwich beam by employing the high-order sinusoidal shear deformation theory and used the modified Voigt mixture rule to approximate the temperature-dependent material properties of porous FGMs. Moreover, they considered the physical neutral plane of FGM sandwich beams to reflect the actual condition of the structures and simplify the calculation. Aria and Friswell (2019) investigated hygro-thermal behaviour of functionally graded (FG) sandwich microbeams based on nonlocal elasticity theory. They considered temperature-dependent material properties for the FG microbeam, which are assumed to change continuously through the thickness based on the power-law form. Emdadi *et al.* (2019) studied the free vibration analysis of annular sandwich plates with various functionally graded (FG) porous cores and carbon nanotubes reinforced composite (CNTRC) facesheets based on modified couple stress theory (MCST) and first order shear deformation theories (FSDT). They considered the annular sandwich plate composed of two face layers and a FG porous core layer which contains different porosity distributions. Saidi *et al.* (2019) presented the vibration and stability analyses of FG reinforced porous plates with piezoelectric layers under supersonic flow. Amir (2019) demonstrated orthotropic patterns of visco-Pasternak foundation in nonlocal vibration of orthotropic graphene sheet under thermo-magnetic fields based on new first-order shear deformation theory. Sofiyev (2019) considered an exhaustive review of the literature on the vibration and buckling of functionally graded materials (FGMs), functionally graded conical shells (FGCSs), functionally graded layered conical shells (FGLCSs), and functionally graded sandwich-conical shells (FGSCSs). Ghannadpour *et al.* (2019) presented nonlinear and post-buckling behaviors of internally cracked FG plates subjected to uniaxial compressive loading. They modelled the crack by decomposing the entire domain of the plate into several sub-plates and therefore, a plate decomposition technique is applied. Some researchers worked about experimental results to obtain the mechanical properties of carbon nanotubes reinforced composite (Mohammadimehr *et al.* 2018a), CFFT with and without FRP (Khan *et al.* 2019), the effect of CFRP on the beam (Xie *et al.* 2019), VHSC encased composite stub column under compression and end moment (Huang *et al.* 2019).

In this paper, hydro-thermo-mechanical biaxial buckling analysis of sandwich micro-plate with an orthotropic core and piezoelectric nanocomposite face sheets is investigated based on FSDT and MSGT. Piezoelectric layers reinforced by carbon and boron-nitride nanotubes (CNTs and BNNTs) under temperature-dependent and hydro material properties on the elastic foundations are considered. The first order shear deformation theory (FSDT) is adopted to model micro sandwich plate and to apply size dependent effects from modified strain gradient theory. Using the minimum total potential energy principle, the governing equations are obtained and then solved by analytical method.

## 2. Governing equations of sandwich microplate

Fig. 1 shows a schematic view of sandwich micro-plate with an orthotropic & isotropic cores and piezoelectric nanocomposite face sheets that are three-layers sandwich rectangular micro-sheet. As shown in the figure, the microstructure core in this section is considered as soft material (Divinycell H60) and orthotropic with a thickness of  $h_c$ .

Also, each of the lower and upper facesheets, with thicknesses  $h_b$  and  $h_t$ , are made of polymeric composite (PmPV) and piezoelectric materials as single-wall carbon nanotubes (SWCNTs) and boron nitride nanotubes (SWBNNT).

In the buckling analysis and microstructure stability, the equivalent properties of composite materials composed of the piezoelectric material and carbon and boron nitride nanotube as reinforcement. Using representative volume element (RVE) of micromechanical approach as well as the buckling of the structure are the equivalent properties of the composite procedures composed of the polymer and reinforced by carbon nanotubes are obtained from to the extended rule of mixture.

First, the equivalent properties for piezoelectric layer are expressed on the basis of the micromechanical approach (Mohammadimehr *et al.* 2016d)

$$C_{11i} = \frac{q_{11\_SWNT} q_{11m}}{(V^i_{SWNT} q_{11m} + (1 - V^i_{SWNT}) q_{11SWNT})}$$

$$C_{12i} = C_{11i} \left( \frac{V^i_{SWNT} q_{12SWNT}}{q_{11SWNT}} + \frac{(1 - V^i_{SWNT}) q_{12m}}{q_{11m}} \right)$$

$$C_{22i} = V^i_{SWNT} q_{22SWNT} + (1 - V^i_{SWNT}) q_{11m}$$

$$C_{66i} = \frac{q_{66SWNT} q_{66m}}{(V^i_{SWNT} q_{66SWNT} + (1 - V^i_{SWNT}) q_{66m})}$$

$$C_{44i} = C_{66i} \quad C_{55i} = C_{66i}$$
(1)

$$e_{24i} = (1 - V^i_{SWNT}) e_{24m} + V^i_{SWNT} e_{24SWNT}$$

$$e_{32i} = (1 - V^i_{SWNT}) e_{32m} + V^i_{SWNT} e_{32SWNT}$$

$$e_{31i} = C_{11i} \left( \left( \frac{(1 - V^i_{SWNT}) e_{31SWNT}}{q_{11SWNT}} \right) + \left( \frac{V^i_{SWNT} e_{31m}}{q_{11m}} \right) \right)$$
(2)

$$e_{15i} = \frac{e_{15m} e_{15\_SWNT}}{((1 - V^i_{SWNT}) e_{15m} + V^i_{SWNT} e_{15\_SWNT})}$$

$$\eta_{11i} = (1 - V^i_{SWNT}) \eta^*_{11m} + V^i_{SWNT} \eta^*_{11SWNT}$$

$$\eta_{22i} = (1 - V^i_{SWNT}) \eta^*_{22m} + V^i_{SWNT} \eta^*_{22SWNT}$$

$$\eta_{33i} = (1 - V^i_{SWNT}) \eta^*_{33m} + V^i_{SWNT} \eta^*_{33SWNT}$$
(3)

$i = t, b$

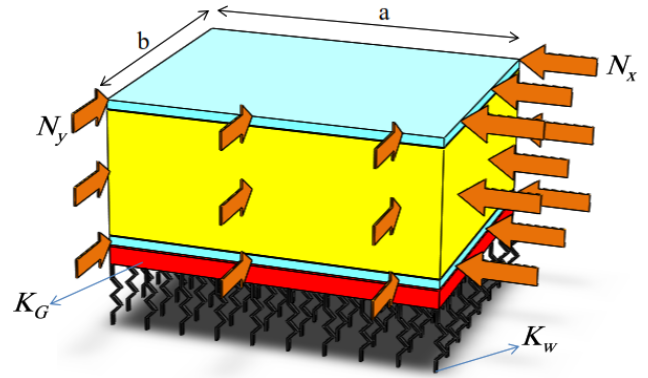


Fig. 1 An schematic view of sandwich micro plates reinforced by FG-NTs subjected to in-plane loading

Eqs. (1)-(3) denote the equivalent properties for elastic constants, the piezoelectric and the dielectric in the facesheet layers, respectively, that are obtained based on micro-mechanical approach.

The relationship (4) is related to the distributions of the nanotube in the upper facesheet layer of the microstructure (Alashti and Khorsand 2012)

$$V^t_{SWNT} \begin{cases} V^*_{SWNT} & UD \\ 2 \left( 2 \frac{|z - (hc + h)|}{2h_t} \right) V^*_{SWNT} & FG - X \\ 2 \left( 1 - 2 \frac{|z - (hc + h)|}{2h_t} \right) V^*_{SWNT} & FG - O \\ \left( 1 + 2 \frac{z - (hc + h)}{2h_t} \right) V^*_{SWNT} & FG - V \end{cases} \quad (4)$$

where  $V^*_{CNT} = \frac{w_{CNT}}{w_{CNT} + \frac{\rho_{CNT}}{\rho_m}(1 - w_{CNT})}$ .  $w_{CNT}$  is the mass fraction of CNT in the composite plate, and  $\rho_m$  and  $\rho_{CNT}$  are the densities of the matrix and CNT, respectively.

The distributions of the nanotubes in the lower facesheet layer is given by the relation (5).

$$V^b_{SWNT} \begin{cases} V^*_{SWNT} & UD \\ 2 \left( 2 \frac{|z + (hc + h)|}{2h_b} \right) V^*_{SWNT} & FG - X \\ 2 \left( 1 - 2 \frac{|z + (hc + h)|}{2h_b} \right) V^*_{SWNT} & FG - O \\ \left( 1 + 2 \frac{z + (hc + h)}{2h_b} \right) V^*_{SWNT} & FG - V \end{cases} \quad (5)$$

Also  $V_{SWNT}$  and  $V_m$  are the SWNT and matrix volume fractions, respectively and we have

$$V_m + V_{SWNT} = 1 \quad (6)$$

For microstructure buckling of polymeric layers and nano-carbon reinforced structures, the equivalent properties are calculated using the extended rule of mixture, which is presented in accordance with relations (7) to (10) (Mohammadimehr *et al.* 2018b, Mohammadimehr and Shahedi 2016).

$$E_{11} = \eta_1 V_{CNT} E_{11_{CNT}} + V_m E_m \quad (7)$$

$$\frac{\eta_2}{E_{22}} = \frac{V_{CNT}}{E_{22_{CNT}}} + \frac{V_m}{E_m} \quad (8)$$

$$\frac{\eta_3}{G_{12}} = \frac{V_{CNT}}{G_{12_{CNT}}} + \frac{V_m}{G_m} \quad (9)$$

$$\rho = V_{CNT} \rho_{CNT} + V_m \rho_m \quad (10)$$

$$v_{12} = V_{CNT}^* v_{12}^{CNT} + V_m v_m^m$$

where  $E_{22_{CNT}}$ ,  $E_{11_{CNT}}$  and  $G_{12_{CNT}}$  are the Young's modulus and shear modulus of the single-walled carbon nanotubes, respectively.  $E_m$  and  $G_m$  are the corresponding properties of the polymer matrix and  $\eta_i$  ( $i = 1, 2, 3$ ) are the CNT efficiency parameters respectively. Also,  $V_{CNT}$  and  $V_m$  are the CNT and matrix volume fractions and are related as follows

$$V_{CNT} + V_m = 1 \quad (11)$$

Fig. 2 shows various configurations of nanotubes (NTs) reinforced composite face sheets including (a) uniform distribution (UD)-carbon nanotube reinforced composite (CNTRC) (b) FG-X CNTRC (c) FG-OCNTRC (d) FG-V CNTRC.

In this paper, the displacement fields are defined on the basis of the first-order shear deformation theory (FSDT) as follows

$$\begin{aligned} u(x, y, z, t) &= z\varphi_x(x, y, t) \\ v(x, y, z, t) &= z\varphi_y(x, y, t) \\ w(x, y, z, t) &= w(x, y, t) \end{aligned} \quad (12)$$

where  $w$  are displacement in  $z$  direction.  $\varphi_x$  and  $\varphi_y$  are the rotation around  $x$  and  $y$  directions, respectively.

Therefore, the strain-displacement (kinematic) relations for the sandwich microstructure are obtained in the following form (Ventsel and Krauthammer 2001)

$$\begin{aligned} \varepsilon_{xx} &= \frac{\partial}{\partial x} u(x, y, z, t) \\ \varepsilon_{yy} &= \frac{\partial}{\partial y} v(x, y, z, t) \\ \gamma_{xy} &= \frac{\partial}{\partial y} u(x, y, z, t) + \frac{\partial}{\partial x} v(x, y, z, t) \\ \gamma_{xz} &= \frac{\partial}{\partial z} u(x, y, z, t) + \frac{\partial}{\partial x} w(x, y, z, t) \\ \gamma_{yz} &= \frac{\partial}{\partial z} v(x, y, z, t) + \frac{\partial}{\partial y} w(x, y, z, t) \end{aligned} \quad (13)$$

Using Hook's law, stress-strain relations for core can be stated as follows

$$\begin{cases} \sigma_{xx} = Q_{11}\varepsilon_{xx} + Q_{12}\varepsilon_{yy} \\ \sigma_{yy} = Q_{21}\varepsilon_{xx} + Q_{22}\varepsilon_{yy} \\ \sigma_{xy} = Q_{66}\gamma_{xy}, \sigma_{xz} = Q_{55}\gamma_{xz}, \sigma_{yz} = Q_{44}\gamma_{yz} \end{cases} \quad (14)$$

where  $\sigma_{ij}$  and  $\varepsilon_{ij}$  are the stress, strain components. Also,  $Q_{ij}$  is the reduced elastic constant for core which can be expressed as follows (Mohammadimehr *et al.* 2018c)

$$\begin{aligned} Q_{11} &= \frac{E}{1-\nu^2} & Q_{22} &= Q_{11} \\ Q_{12} &= \frac{\nu E}{1-\nu^2} & Q_{21} &= Q_{12} \\ Q_{66} &= \frac{E}{2(1+\nu)} \\ Q_{55} &= Q_{66} & Q_{44} &= Q_{66} \end{aligned} \quad (15)$$

In order to obtain the governing equations for micro sandwich plate with piezoelectric facesheet and composite-reinforced with carbon and boron-nitride nanotubes, the principle of minimum total potential energy is used. In this method, the total potential energy is obtained from the sum of the energy of the strain potential and the work done by

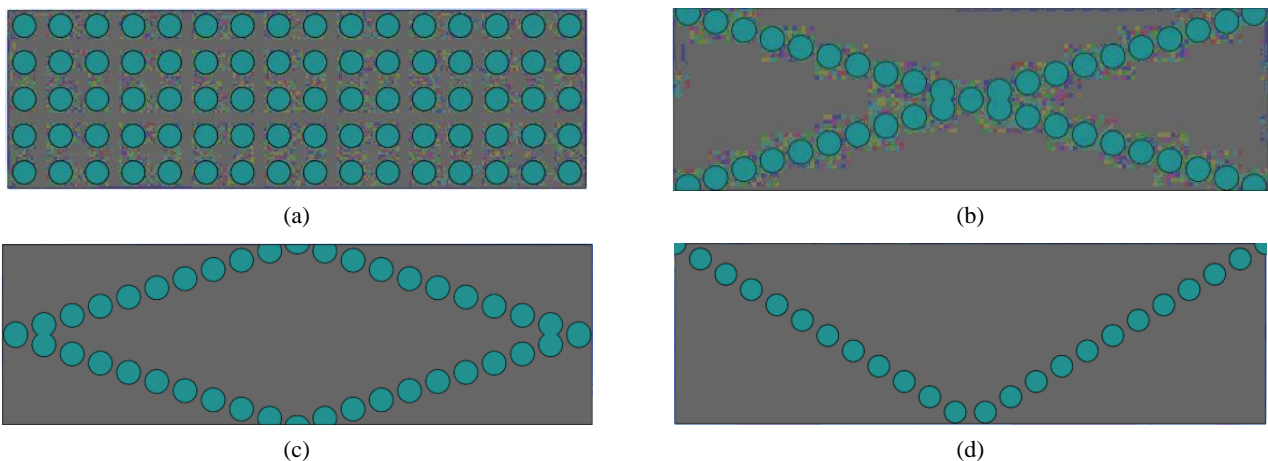


Fig. 2 Configurations of NTs reinforced composite face sheets. (a) UD; (b) FG-X; (c) FG-O; (d) FG-V

the external forces in the following form

$$\prod = (U + V) \tag{16}$$

$$\delta \Pi = 0 \rightarrow \delta U + \delta V = 0$$

where U and V are strain energy and the work done by the external forces, respectively.

Work done by the external loads can be stated as

$$V = V^{transverseload} + V^{elastic} + V^{Buck} \tag{17}$$

In the above relation,  $V^{transverseload}$ ,  $V^{elastic}$  and  $V^{Buck}$  are the transvers load, the elastic foundation and the buckling load due to the presence of  $N_x$  and  $N_y$  that is defined as follows (Nasihatgozar *et al.* 2016)

$$\delta V^{Buck} = \int \left[ N_x^0 \left( \frac{\partial^2 w}{\partial x^2} \right) + N_y^0 \left( \frac{\partial^2 w}{\partial y^2} \right) \right] \delta w dA \tag{18}$$

In the relationship (18),  $N_x^0$  and  $N_y^0$  are in-plane forces for micro sandwich plate.

The work done due to elastic foundation is considered as follows

$$\begin{aligned} & \delta V^{transverseload\&Elastic} \\ &= - \int A \left\{ \left[ K_w w(x, y) - K_G \left( \frac{\partial^2 w(x, y)}{\partial x^2} + \frac{\partial^2 w(x, y)}{\partial y^2} \right) \right] \delta w \right\} dA \tag{19} \\ &+ \int A [q \delta w] dA \end{aligned}$$

By substituting Eqs. (18) and (19) into Eq. (17), we have the sum of the obtained relations from the transvers load and elastic foundation and buckling load (relationship (18) and (19)) that is stated as follows

$$\begin{aligned} \delta V = & \int A \left\{ \left[ K_w w(x, y) - K_G \left( \frac{\partial^2 w(x, y)}{\partial x^2} + \frac{\partial^2 w(x, y)}{\partial y^2} \right) \right] \delta w \right\} dA \tag{20} \\ &+ \int A [q \delta w] dA + \int \left[ N_x^0 \left( \frac{\partial^2 w}{\partial x^2} \right) + N_y^0 \left( \frac{\partial^2 w}{\partial y^2} \right) \right] \delta w dA \end{aligned}$$

The variation of strain energy based on modified strain gradient theory (MSGT) for the micro sandwich piezoelectric plate can be obtained as follows (Mohammadimehr *et al.* 2016d)

$$\begin{aligned} \delta U = & \int_V (\sigma_{ij} \delta \varepsilon_{ij} + p_i \delta \gamma_i + \tau_{ijk}^{(1)} \delta \eta_{ijk}^{(1)} \\ &+ m_{ij}^{(s)} \delta \chi_{ij}^{(s)} - D_i \delta E_i) dV \tag{21} \end{aligned}$$

where  $\eta_{ijk}$ ,  $\chi_{ij}$  and  $\gamma_i$  are deviatoric stretch gradient tensor, symmetric rotation gradient tensor and dilatation

Table 1 The values of three material length scale parameters for classical, modified couple stress and modified strain gradient theories

Theory	$l_0$ ( $\mu m$ )	$l_1$ ( $\mu m$ )	$l_2$ ( $\mu m$ )
CPT	0	0	0
MCST	0	0	17.6
MSGT	17.6	17.6	17.6

gradient vector, respectively, and  $D_i$  and  $E_i$  denote the electric displacement and the electric field, respectively that is defined in Appendix A.

Table 1 shows the values of three material length scale parameters for classical, modified couple stress and modified strain gradient theories, respectively.

The electric field is considered in two ways according to the relations (22) and (23) for the above mentioned structure.

For the upper facesheet

$$\begin{cases} \psi^t(x, y, z, t) = -\psi(x, y, t) \cos \left( \frac{\pi \left( z - \frac{1}{2}hc - \frac{1}{2}h \right)}{h} \right) \\ E_i = -\frac{\partial \tilde{\varphi}_E(x, y, z)}{\partial x_i} \end{cases} \tag{22}$$

For the bottom facesheet

$$\begin{cases} \psi^b(x, y, z, t) = -\psi(x, y, t) \cos \left( \frac{\pi \left( z + \frac{1}{2}hc + \frac{1}{2}h \right)}{h} \right) \\ E_i = -\frac{\partial \tilde{\varphi}_E(x, y, z)}{\partial x_i} \end{cases} \tag{23}$$

The proposed structural relations are defined as relations (23)-(25) for composite, piezoelectric facesheet and core, respectively.

There are two different structures such as a microstructure with polymer composite layers reinforced by nanotubes and a piezoelectric microstructure reinforced with carbon and boron nitride nanotubes.

$$\begin{Bmatrix} \sigma_{xx}^i \\ \sigma_{yy}^i \\ \tau_{zy}^i \\ \tau_{xz}^i \\ \tau_{xy}^i \end{Bmatrix} = \begin{bmatrix} C_{11}^i & C_{12}^i & 0 & 0 & 0 \\ C_{12}^i & C_{22}^i & 0 & 0 & 0 \\ 0 & 0 & C_{44}^i & 0 & 0 \\ 0 & 0 & 0 & C_{55}^i & 0 \\ 0 & 0 & 0 & 0 & C_{66}^i \end{bmatrix} \begin{Bmatrix} \varepsilon_x - \alpha_x \Delta T - \beta_x \Delta H \\ \varepsilon_y - \alpha_y \Delta T - \beta_y \Delta H \\ \gamma_{zy} \\ \gamma_{xz} \\ \gamma_{xy} \end{Bmatrix} \quad i = t, b \tag{24}$$

$$\begin{cases} \sigma_{xx}^i = C_{11}(z) \varepsilon_{xx}^i + C_{12}(z) \varepsilon_{yy}^i + e_{31}(z) E_z^i \\ \sigma_{yy}^i = C_{12}(z) \varepsilon_{xx}^i + C_{22}(z) \varepsilon_{yy}^i + e_{32}(z) E_z^i \\ \sigma_{xy}^i = C_{66}(z) \gamma_{xy}^i \\ \sigma_{yz}^i = C_{44}(z) \gamma_{yz}^i + e_{24}(z) E_x^i \\ \sigma_{xz}^i = C_{55}(z) \gamma_{xz}^i + e_{15}(z) E_x^i \\ D_x^i = e_{15}(z) \gamma_{xz}^i + \eta_{11}(z) E_x^i \\ D_y^i = e_{24}(z) \gamma_{yz}^i + \eta_{22}(z) E_y^i \\ D_z^i = e_{31}(z) \varepsilon_{xx}^i + e_{32}(z) \varepsilon_{yy}^i + \eta_{33}(z) E_z^i \end{cases} \quad i = t, b \tag{25}$$

$$\begin{cases} E_{11}v_{21} = E_{22}v_{12} \\ C_{11} = \frac{E_{11}}{1 - v_{12}v_{21}} \\ C_{12} = \frac{v_{21}E_{11}}{1 - v_{12}v_{21}} \\ C_{22} = \frac{E_{22}}{1 - v_{12}v_{21}} \\ C_{44} = G_{23}, C_{55} = G_{13}, C_{66} = G_{12} \end{cases} \quad (26)$$

Using the minimum total potential energy, the governing equations for micro sandwich plate with an orthotropic core and piezoelectric/polymeric nanocomposite face sheets based on FSDT and MSGT are obtained.

$$\begin{aligned} \delta\varphi_x: & -\frac{\partial}{\partial x}M_{xx} - \frac{\partial}{\partial y}M_{xy} + N_{0xz} + \frac{\partial^2}{\partial x^2}P_{1x} \\ & + \frac{\partial^2}{\partial x \partial y}P_{1y} - \frac{\partial}{\partial x}P_{0z} + \frac{2}{5}\frac{\partial^2}{\partial x^2}T_{1xxx} \\ & - \frac{1}{5}\frac{\partial^2}{\partial y^2}T_{1xxx} + 3\left(\frac{8}{15}\frac{\partial^2}{\partial x \partial y}T_{1xxy}\right) \\ & + 3\left(-\frac{8}{15}\frac{\partial}{\partial x}T_{0xxz}\right) + 6\left(-\frac{1}{3}\frac{\partial}{\partial y}T_{0xyz}\right) \\ & + 3\left(\frac{4}{15}\frac{\partial^2}{\partial y^2}T_{1xyy} - \frac{1}{5}\frac{\partial^2}{\partial x^2}T_{1xyy}\right) \\ & + 3\left(-\frac{1}{5}\frac{\partial^2}{\partial x^2}T_{1xzz} - \frac{1}{15}\frac{\partial^2}{\partial y^2}T_{1xzz}\right) \\ & - \frac{2}{5}\frac{\partial^2}{\partial x \partial y}T_{1yyy} + 3\left(\frac{2}{15}\frac{\partial}{\partial x}T_{0yyz}\right) \\ & + 3\left(-\frac{2}{15}\frac{\partial^2}{\partial x \partial y}T_{1yzz}\right) + \frac{2}{5}\frac{\partial}{\partial x}T_{0zzz} \\ & - \frac{1}{2}\frac{\partial}{\partial y}R_{0y} + \frac{1}{2}\frac{\partial}{\partial y}R_{0z} - \frac{1}{4}\frac{\partial}{\partial x}R_{0xy} \\ & - \frac{1}{4}\frac{\partial^2}{\partial x \partial y}R_{1xz} - \frac{1}{4}\frac{\partial^2}{\partial y^2}R_{1yz} = 0 \end{aligned} \quad (27)$$

$$\begin{aligned} \delta w: & -\frac{\partial}{\partial x}N_{0xz} - \frac{\partial}{\partial y}N_{0zy} \\ & + 3\left(\frac{4}{15}\frac{\partial^2}{\partial x^2}T_{0xxz} - \frac{1}{15}\frac{\partial^2}{\partial y^2}T_{0xxz}\right) \\ & + \frac{6}{3}\frac{\partial^2}{\partial x \partial y}T_{0xyz} \\ & + 3\left(\frac{4}{15}\frac{\partial^2}{\partial y^2}T_{0yyz} - \frac{1}{15}\frac{\partial^2}{\partial x^2}T_{0yyz}\right) \\ & - \frac{1}{5}\frac{\partial^2}{\partial x^2}T_{0zzz} - \frac{1}{5}\frac{\partial^2}{\partial y^2}T_{0zzz} + \frac{1}{2}\frac{\partial^2}{\partial x \partial y}R_{0x} \\ & - \frac{1}{2}\frac{\partial^2}{\partial x \partial y}R_{0y} + \frac{1}{4}\frac{\partial^2}{\partial y^2}R_{0xy} - \frac{1}{4}\frac{\partial^2}{\partial x^2}R_{0xy} \\ & + K_w \cdot w(x, y, t) - K_g \cdot \frac{\partial^2}{\partial x^2}w(x, y, t) \\ & - K_g \cdot \frac{\partial^2}{\partial y^2}w(x, y, t) - q(x, y) \\ & + N_x \left( \frac{\partial^2}{\partial x^2}w(x, y, t) + t \frac{\partial^2}{\partial y^2}w(x, y, t) \right) = 0 \end{aligned} \quad (28)$$

$$\begin{aligned} \delta\varphi_y: & -\frac{\partial}{\partial y}M_{yy} - \frac{\partial}{\partial x}M_{xy} + N_{0zy} + \frac{\partial^2}{\partial x \partial y}P_{1x} \\ & + \frac{\partial^2}{\partial y^2}P_{1y} - \frac{\partial}{\partial y}P_{0z} - \frac{2}{5}\frac{\partial^2}{\partial x \partial y}T_{1xxx} \\ & + 3\left(\frac{4}{15}\frac{\partial^2}{\partial x^2}T_{1xxy} - \frac{1}{5}\frac{\partial^2}{\partial y^2}T_{1xxy}\right) \\ & + 3\left(\frac{2}{15}\frac{\partial}{\partial y}T_{0xxz}\right) - 6\left(\frac{1}{3}\frac{\partial}{\partial x}T_{0xyz}\right) \\ & + 3\left(\frac{8}{15}\frac{\partial^2}{\partial x \partial y}T_{1xyy}\right) - 3\left(\frac{2}{15}\frac{\partial^2}{\partial x \partial y}T_{1xzz}\right) \\ & + \frac{2}{5}\frac{\partial^2}{\partial y^2}T_{1yyy} - \frac{1}{5}\frac{\partial^2}{\partial x^2}T_{1yyy} - 3\left(\frac{8}{15}\frac{\partial}{\partial y}T_{0yyz}\right) \\ & - 3\left(\frac{1}{5}\frac{\partial^2}{\partial y^2}T_{1yzz} + \frac{1}{15}\frac{\partial^2}{\partial x^2}T_{1yzz}\right) + \frac{2}{5}\frac{\partial}{\partial y}T_{0zzz} \\ & + \frac{1}{2}\frac{\partial}{\partial x}R_{0x} - \frac{1}{2}\frac{\partial}{\partial x}R_{0z} + \frac{1}{4}\frac{\partial}{\partial y}R_{0xy} \\ & + \frac{1}{4}\frac{\partial^2}{\partial x^2}R_{1xz} + \frac{1}{4}\frac{\partial^2}{\partial x \partial y}R_{1yz} = 0 \end{aligned} \quad (29)$$

$$\delta\psi: \quad \frac{\partial}{\partial x}D_{1x} + \frac{\partial}{\partial y}D_{1y} + D_{1z} = 0 \quad (30)$$

where  $N_{0xz}$ ,  $N_{0zy}$ ,  $M_{xx}$ ,  $M_{yy}$ ,  $M_{xy}$  are defined the force and torque results, as well as the constants defined for simplifying the equations in Appendix (B).

### 3. Solution of basic equations

Navier's type solution for the micro sandwich piezoelectric polymeric nanocomposite rectangular plates with all edges simply supported boundary conditions are considered as follows

$$\begin{aligned} w(x, y) &= \sum_{n=1}^{\infty} \sum_{m=1}^{\infty} w_{mn} \sin\left(\frac{m\pi x}{a}\right) \sin\left(\frac{n\pi y}{b}\right) \\ \varphi_x(x, y) &= \sum_{n=1}^{\infty} \sum_{m=1}^{\infty} A_{mn} \cos\left(\frac{m\pi x}{a}\right) \sin\left(\frac{n\pi y}{b}\right) \\ \varphi_y(x, y) &= \sum_{n=1}^{\infty} \sum_{m=1}^{\infty} B_{mn} \sin\left(\frac{m\pi x}{a}\right) \cos\left(\frac{n\pi y}{b}\right) \\ \psi(x, y) &= \sum_{n=1}^{\infty} \sum_{m=1}^{\infty} \psi_{mn} \cdot \sin\left(\frac{m\pi x}{a}\right) \sin\left(\frac{n\pi y}{b}\right) \end{aligned} \quad (31)$$

In (31),  $w_{mn}$ ,  $A_{mn}$ ,  $B_{mn}$ ,  $\psi_{mn}$  are Fourier's constant coefficients. In addition,  $m$  and  $n$  are wave numbers in two directions of the longitudinal and transverse directions, respectively. By replacing the relationship variables (31) into the governing equations, following matrix form for micro sandwich plate is obtained as follows

$$([K] - \lambda^2[S])\{\tilde{C}\} = 0 \quad (32)$$

Table 2 The geometric and mechanical properties of the plate for validation (Lei *et al.* 2013, Timohsneko and Gere 1961)

Specifications								
$a(m)$	$b(m)$	$h(m)$	$\nu$	$\phi$	$K_w$	$K_G$	$q$	$E(GPa)$
0.254	0.254	0.00508	0.3	0	0	0	0	20.68427188

Table 3 Comparison the obtained results for present work and the other literatures

Mode number	Present work	Lei <i>et al.</i> (2013)	Analytical (Timohsneko and Gere 1961)
1	39.40	39.47	39.47
2	61.39	60.48	61.68
3	108.64	105.39	109.65

Table 4 Geometric and mechanical properties of sandwich micro-plate with isotropic and orthotropic core

Geometry									
$h = l$	$h_c$	$H$	$b = a$	$h_{t,b}$					
(Base size)	(Core thickness)	(Total thickness)	(Length and width)	(Thickness of the facesheets)					
$17.6 \times 10^{-6}m$	$5h$	$h_c + (2h)$	$10H$	$h$					
Mechanical properties of the core									
Isotropic (Devynycell H200)			Orthotropic (Mohammadimehr <i>et al.</i> 2018c)						
$E(Pa)$	$\nu$	$\rho(Kg/m^3)$	$E_{11}(Pa)$	$E_{22}(Pa)$	$\nu_{12}$	$\nu_{21}$	$\rho(Kg/m^3)$	$G_{12}(Pa)$	$G_{13} = G_{23}(Pa)$
$277 \times 10^6$	0.3	200	$7.347 \times 10^9$	$8.816 \times 10^9$	0.25	0.3	1000	$3.159 \times 10^9$	$4.218 \times 10^9$

Finally, the resulting algebraic equation system is solved in the form of an eigen-value problem in the form of relation (32). In the above relation,  $K$  and  $S$  are stiffness and buckling matrices, respectively.

#### 4. Numerical results and discussion

In this section, we examine the effects of different parameters on the buckling of the micro sandwich plate in

the form of tables and figures. In the analysis, all conditions such as geometric, mechanical, and loading on facesheets are assumed to be the same.

In Table 2, the geometric and mechanical properties of the plate for validation are considered.

Two types of core including isotropic and orthotropic are considered for the present work. The first type core is an orthotropic material. Five isotropic materials such as *Devynycell H30, H45, H60, H100* and *H200* are considered for core.

Table 5 Mechanical properties of a polymeric matrix (PMMA) (Sharif Zarei *et al.* 2018, Mohammadimehr and Mostafavifar 2016)

Mechanical properties of Matrix				
$E_m(GPa)$	$\nu_m$	$\rho_m \left(\frac{kg}{m^3}\right)$	$\alpha_m \left(\frac{10^{-6}^\circ}{C}\right)$	$\beta_m \left(\frac{10^{-3}^\circ}{wt} \cdot H_2O\right)$
$(3.51 - 0.0034T - 0.142H)$	0.34	1200	45.0	2.68

Table 6 Mechanical and thermal properties of carbon nanotubes (Mohammadimehr *et al.* 2016c)

$K$	$E_{11}^{CNT}(TPa)$	$E_{22}^{CNT}(TPa)$	$G_{12}^{CNT}(TPa)$	$\alpha_{11}^{CNT} \left(\times \frac{10^{-6}}{K}\right)$	$\alpha_{22}^{CNT} \left(\times \frac{10^{-6}}{K}\right)$
300	5.6664	7.0800	1.9445	3.4548	5.1682
500	5.5308	6.9348	1.9643	4.5361	5.0189
700	5.4744	6.8641	1.9644	4.6677	4.8943

According to Table 3, the obtained results for present work and the other literatures (Lei *et al.* 2013 and Timoshenko and Gere 1961) compare each other that there is a good agreement between them.

Table 4 shows the geometric and mechanical properties of sandwich micro-plate with isotropic and orthotropic core.

As mentioned earlier, the used facesheets in the present work are two cases:

Case 1: Consider nano composite material with a polymeric matrix (PMMA) reinforced by carbon nanotubes

Table 7 Performance parameters for different volume fractions of carbon nanotubes

$V_{CNT}^*$	$\eta_1$	$\eta_2$	$\eta_3$
0.12	0.137	1.022	0.715
0.17	0.142	1.626	1.138
0.28	0.141	1.585	1.109

that the mechanical properties are given in Tables 5 and 6 ( $T = T_0 + \Delta T$ ,  $T_0 = 300^\circ K$ )

$$H = H_0 + \Delta H, H_0 = 0 \text{ } \overset{\circ}{\underset{\circ}{H_2O}}$$

Performance parameters for various volume fractions of carbon nanotubes are presented in Table 7.

Case 2: Consider nano composite material with a piezoelectric (PVDF matrix) reinforced by carbon and boron nitride nanotubes that the mechanical properties are given in Table 8.

The dimensionless critical buckling load of the sandwich microplate versus core to the facesheets thickness ratio for different distributions of carbon nanotubes including uniform distribution (UD), functionally graded (FG)-X, FG-O and FG-V carbon nanotube reinforced composite (CNTRC) with various cores: (a) isotropic (Devineycell H200); (b) orthotropic is shown in Figs. 3(a) and (b). With increasing core to facesheet thickness ratio

Table 8 Mechanical properties of nanotubes and piezoelectric (PVDF matrix) (Mohammadimehr *et al.* 2016d)

SWCNT	SWBNNT	PVDF(matrix)
$q_{11}^{SWCNTs} = 5.8249TPa$	$q_{11}^{SWBNNTs} = q_{22}^{SWBNNTs} = 2035GPa$	$q_{11}^m = q_{22}^m = 8.5779GPa$
$q_{22}^{SWCNTs} = 7.3037TPa$	$q_{12}^{SWBNNTs} = 692 GPa$	$q_{12}^m = 1.544GPa$
$q_{12}^{SWCNTs} = 1.01937TPa$	$q_{44}^{SWBNNTs} = 672 GPa$	$q_{44}^m = 3.5169GPa$
$q_{44}^{SWCNTs} = 1.9445TPa$	$q_{55}^{SWBNNTs} = q_{66}^{SWBNNTs} = q_{44}^{SWBNNTs}$	$q_{55}^m = q_{66}^m = q_{44}^m$
$q_{55}^{SWCNTs} = q_{44}^{SWCNTs} = q_{66}^{SWCNTs}$	$e_{31}^{SWBNNTs} = 0.95 \frac{C}{m}$	$e_{31}^m = -0.13 \frac{C}{m}$
	$e_{32}^{SWBNNTs} = -0.45 \frac{C}{m}$	$e_{32}^m = -0.45 \frac{C}{m}$
	$e_{24}^{SWBNNTs} = -0.276 \frac{C}{m}$	$e_{24}^m = -0.276 \frac{C}{m}$
	$e_{15}^{SWBNNTs} = -0.009 \frac{C}{m}$	$e_{15}^m = -0.009 \frac{C}{m}$
	$\eta_{11}^{SWBNNTs} = 1.7708e - 10 \frac{F}{m}$	$\eta_{11}^m = 1.1068e - 8 \frac{F}{m}$
	$\eta_{22}^{SWBNNTs} = \eta_{33}^{SWBNNT} = \eta_{11}^{SWBNNTs}$	$\eta_{22}^m = \eta_{33}^m = \eta_{11}^m$

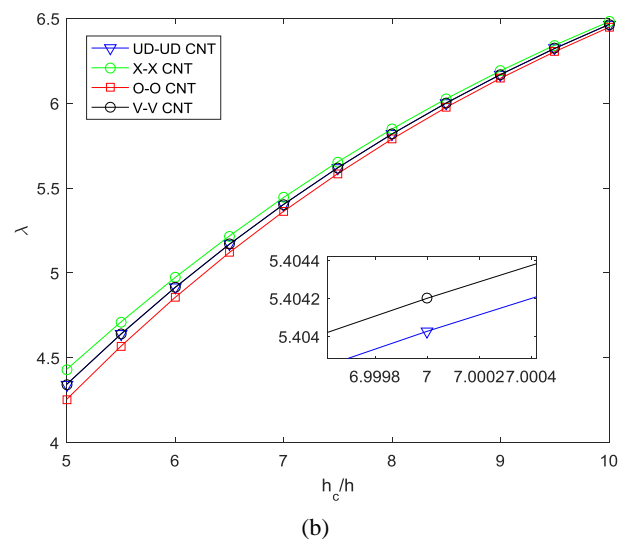
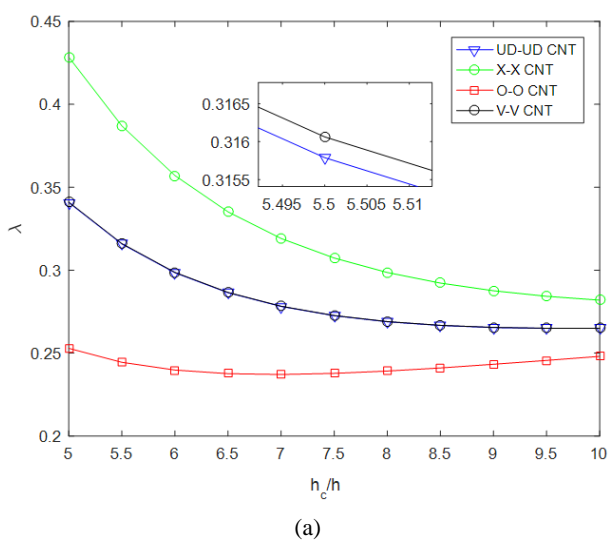


Fig. 3 The dimensionless critical buckling load of the sandwich microplate versus core to the facesheets thickness ratio for different distributions of carbon nanotubes with various cores: (a) isotropic (H200); (b) orthotropic

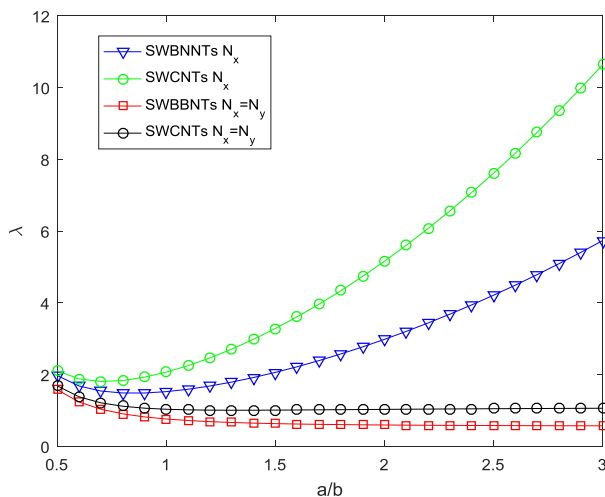


Fig. 4 The influence of biaxial and axial on the dimensionless critical buckling load of the sandwich microplate versus side ratio with isotropic core and piezoelectric facesheets reinforced by carbon and boron nitride nanotubes

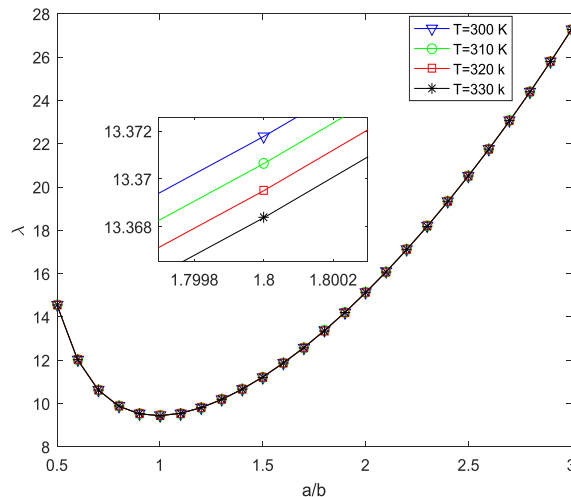


Fig. 6 The influence of temperature changes on the dimensionless critical buckling load for the sandwich microplate versus side ratio with orthotropic core

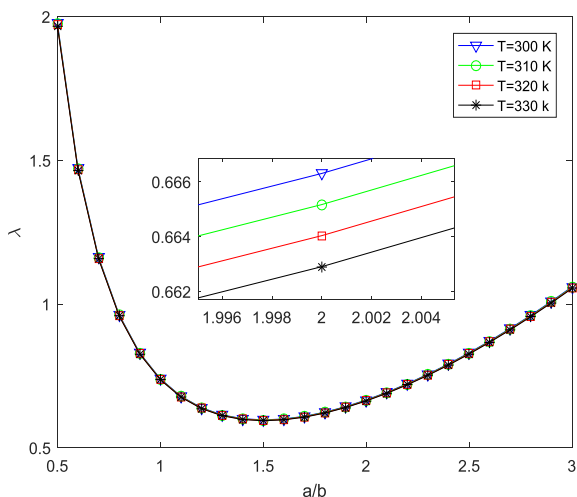


Fig. 5 The influence of temperature changes on the dimensionless critical buckling load for the sandwich microplate versus side ratio with isotropic core

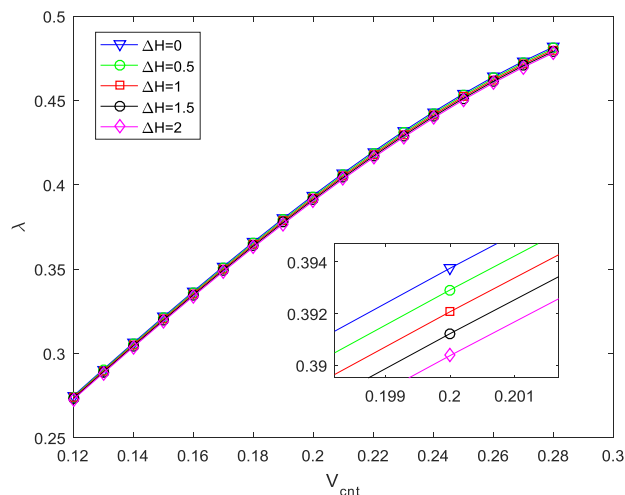


Fig. 7 The dimensionless critical buckling load versus volume fraction of CNT for the sandwich microplate with isotropic core in various moisture changes

$(h_c/h)$  increases the critical buckling load for isotropic core sandwich plate and reduces for the orthotropic core. The critical buckling load of FG-X has the highest value and vice versa for FG-O.

Fig. 4 shows the influence of biaxial and axial on the dimensionless critical buckling load of the sandwich microplate versus side ratio ( $a/b$ ) with isotropic core (Devineycell H200) and piezoelectric facesheets reinforced by single-walled carbon and boron nitride nanotubes (SWCNTs and SWBNTs). It is concluded from this figure that the biaxial critical buckling load is lower than axial critical buckling load for CNT and BNNT. Also, it is seen that the dimensionless critical buckling load for SWBNT is lower than that of for SWCNT in two states including biaxial and axial; while for biaxial state, the obtained results from CNT and BNNT are near to each other with respect to

axial buckling load.

Figs. 5 and 6 illustrated the influences of temperature changes on the dimensionless critical buckling load for the sandwich microplate versus side ratio with isotropic and orthotropic cores, respectively. It is shown from two figures that the difference between two cases such as isotropic and orthotropic cores in lower temperature changes is negligible while in higher values of temperature changes the difference between curves for isotropic core increases but for orthotropic is not noticeable.

The dimensionless critical buckling load versus volume fraction of CNT for the sandwich microplate with orthotropic and orthotropic cores in various moisture changes is plotted in Figs. 7 and 8. It is shown from two figures that the difference between two cases such as isotropic and orthotropic cores in various moisture changes ignores while the dimensionless critical buckling load enhances by increasing of volume fractions of CNT for

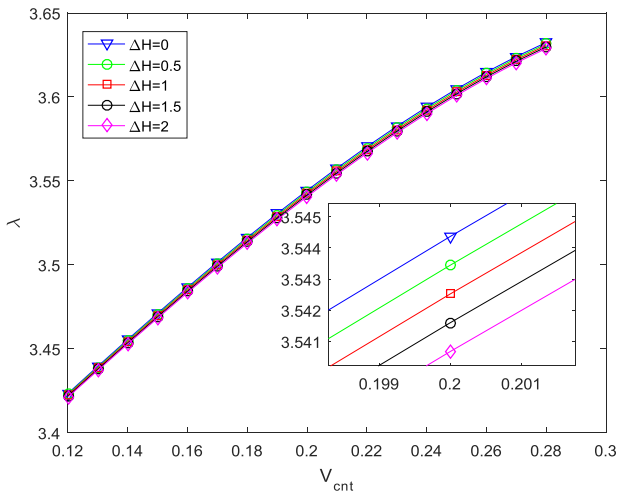


Fig. 8 The dimensionless critical buckling load versus volume fraction of CNT for the sandwich microplate with orthotropic core in various moisture changes

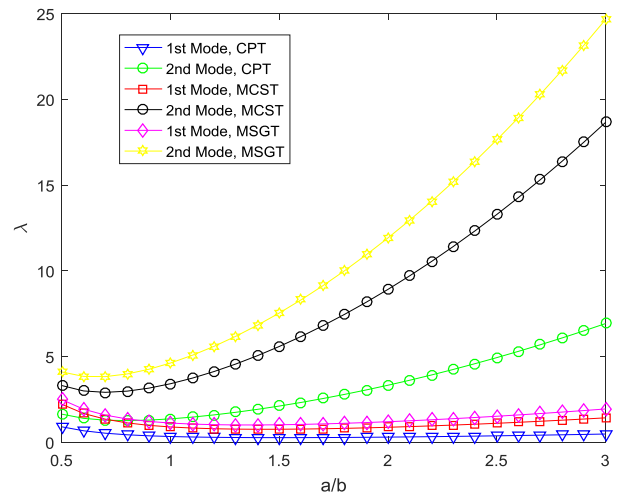
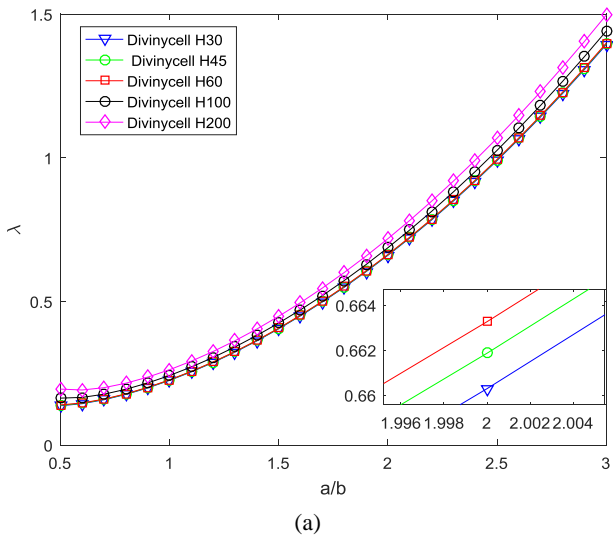
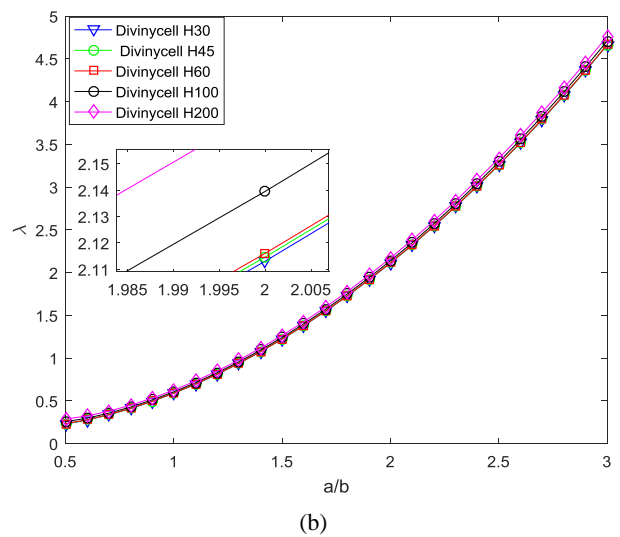


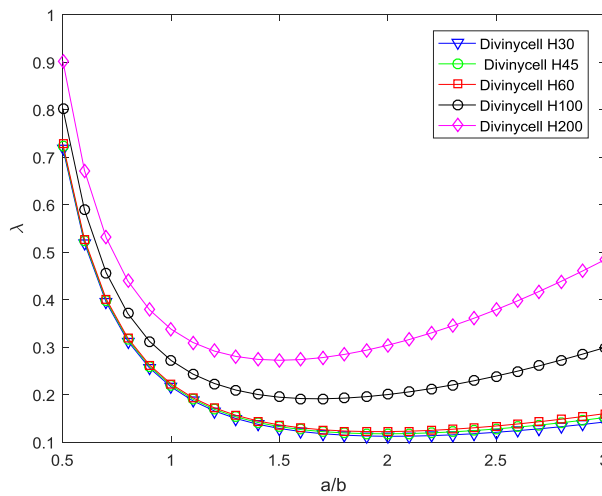
Fig. 9 The dimensionless critical buckling load versus side ratio of the sandwich micro-plate with isotropic core for various size dependent theories



(a)



(b)



(c)

Fig. 10 The influence of various mechanical properties for isotropic core with (a) piezoelectric facesheets reinforced with boron nitride nanotubes; (b) piezoelectric facesheets reinforced with carbon nanotubes; (c) polymeric matrix reinforced by carbon nanotubes

orthotropic and orthotropic cores. It is due to increasing the stiffness of microstructures, when the carbon nanotubes add to polymeric matrix.

In Fig. 9, the effect of various size dependent theories such as classical plate theory (CPT), modified couple stress theory (MCST) and modified strain gradient theory (MSGT) on the dimensionless critical buckling load with isotropic core is investigated. It can be seen that the dimensionless critical buckling load for MSGT is higher than other theories because of this theory considers three material length scale parameter according to Table 1. Also, with increasing the value of axial wave number, the dimensionless critical buckling load increases.

## 5. Conclusions

In this article, the biaxial and axial buckling analysis of micro sandwich plate with an isotropic/orthotropic cores and piezoelectric/polymeric nanocomposite face sheets is investigated. In this research, two cases for core of micro sandwich plate is considered that involve five isotropic Devineycell materials (H30, H45, H60, H100 and H200) and an orthotropic material also two cases for facesheets of micro structure is illustrated that include a piezoelectric matrix (PVDF) reinforced by carbon and boron-nitride nanotubes (CNTs and BNNTs) and a polymeric matrix (PMMA) reinforced by carbon nanotubes (CNTs) under temperature-dependent and hydro material properties on the elastic foundations. Also, different distributions of carbon nanotubes including uniform distribution (UD), functionally graded (FG) carbon nanotube reinforced composite (CNTRC) such as FG-X, FG-O and FG-V are taken into account. The first order shear deformation theory (FSDT) is consider to model sandwich micro plate and to apply size dependent effects from modified strain gradient theory. The governing equations are derived using the minimum total potential energy principle and then solved by analytical method. Also, the effects of different parameters such as size dependent, side ratio, core to facesheet thickness ratio, volume fraction, different distributions of nanotubes, various material properties for cores and facesheets and temperature and humidity changes on the dimensionless critical buckling load are investigated. The obtained results showed that with increasing core to facesheet thickness ratio ( $h_c/h$ ), the critical buckling load for isotropic core sandwich plate increases and reduces for the orthotropic core. The critical buckling load of FG-X has the highest value and vice versa for FG-O. Also, it is concluded from the figure that the biaxial critical buckling load is lower than axial critical buckling load for CNT and BNNT. Also, it is seen that the dimensionless critical buckling load for SWBNNT is lower than that of for SWCNT. It is shown that the difference between two cases such as isotropic and orthotropic cores in lower temperature changes is negligible while in higher values of temperature changes, the difference between curves for isotropic core increases but for orthotropic is not noticeable. It is expressed that the difference between two cases such as isotropic and orthotropic cores in various moisture changes ignores while

the dimensionless critical buckling load enhances by increasing of volume fractions of CNT for orthotropic and orthotropic cores. It is due to increasing the stiffness of microstructures, when the carbon nanotubes add to polymeric matrix. It can be seen that the dimensionless critical buckling load for MSGT is higher than other theories. It is demonstrated that the dimensionless critical buckling load for Devineycell H200 is highest and lowest for H30, because of the mechanical properties for H200 is higher than other states. Also, the obtained results for micro sandwich plate with piezoelectric facesheets reinforced with carbon nanotubes (case b) is higher than other states (cases a and c). The results of this research can be used in aircraft, automotive, shipbuilding industries and biomedicine.

## Acknowledgments

The authors would like to thank the reviewers for their valuable comments and suggestions to improve the clarity of this work. Also, they are thankful to the Iranian Nanotechnology Development Committee for their financial support and the University of Kashan for supporting this work by Grant No. 891238/2.

## References

- Alashti, R.A. and Khorsand, M. (2012), "Three-dimensional dynamo-thermo-elastic of a functionally graded cylindrical shell with piezoelectric layers by DQ-FD coupled", *Int. J. Press. Vessels Pip.*, **96**, 49-67.  
<https://doi.org/10.1016/j.ijpvp.2012.06.006>
- Amir, S. (2019), "Orthotropic patterns of visco-Pasternak foundation in nonlocal vibration of orthotropic graphene sheet under thermo-magnetic fields based on new first-order shear deformation theory", *Proceedings of the Institution of Mechanical Engineers, Part L: Journal of Materials: Design and Applications*, **233**(2), 197-208.  
<https://doi.org/10.1177/1464420716670929>
- Ansari, R., Torabi, J. and Hasrati, E. (2018), "Axisymmetric nonlinear vibration analysis of sandwich annular plates with FG-CNTRC face sheets based on the higher-order shear deformation plate theory", *Aerosp. Sci. Technol.*, **77**, 306-319.  
<https://doi.org/10.1016/j.ast.2018.01.010>
- Aria, A.I. and Friswell, M.I. (2019), "Computational hygro-thermal vibration and buckling analysis of functionally graded sandwich microbeams", *Compos. Part B: Eng.*, **165**, 785-797.  
<https://doi.org/10.1016/j.compositesb.2019.02.028>
- Arshid, E., Kiani, A. and Amir, S. (2019), "Magneto-electro-elastic vibration of moderately thick FG annular plates subjected to multi physical loads in thermal environment using GDQ method by considering neutral surface", *Proceedings of the Institution of Mechanical Engineers, Part L: Journal of Materials: Design and Applications*, p.1464420719832626.  
<https://doi.org/10.1177/1464420719832626>
- Bahaadini, R. and Saidi, A.R. (2019), "Aeroelastic analysis of functionally graded rotating blades reinforced with graphene nanoplatelets in supersonic flow", *Aerosp. Sci. Technol.*, **80**, 381-391. <https://doi.org/10.1016/j.ast.2018.06.035>
- Birman, V. and Kardomateas, G.A. (2018), "Review of current trends in research and applications of sandwich structures", *Compos. Part B: Eng.*, **142**, 221-240.  
<https://doi.org/10.1016/j.compositesb.2018.01.027>

- Emdadi, M., Mohammadimehr, M. and Roustae, Navi B. (2019), "Free vibration of an annular sandwich plate with CNTRC facesheets and FG porous cores using Ritz method", *Adv. Nano Res., Int. J.*, **7**(2), 109-123.  
<https://doi.org/10.12989/anr.2019.7.2.109>
- Ghannadpour, S.A.M., Karimi, M. and Tornabene, F. (2019), "Application of plate decomposition technique in nonlinear and post-buckling analysis of functionally graded plates containing crack", *Compos. Struct.*, **220**, 158-167.  
<https://doi.org/10.1016/j.compstruct.2019.03.025>
- Ghorbanpour Arani, A. and Soleymani, T. (2019), "Size-dependent vibration analysis of a rotating MR sandwich beam with varying cross section in supersonic airflow", *Int. J. Mech. Sci.*, **151**, 288-299. <https://doi.org/10.1016/j.ijmecsci.2018.11.024>
- Ghorbanpour Arani, A., Hashemian, M., Loghman, A. and Mohammadimehr, M. (2011), "Study of dynamic stability of the double-walled carbon nanotubes under axial loading embedded in an elastic medium by the energy method", *J. Appl. Mech. Tech. Phys.*, **52**(5), 815-824.  
<https://doi.org/10.1134/S0021894411050178>
- Ghorbanpour Arani, A., Mobarakeh, M.R., Shams, S. and Mohammadimehr, M. (2012), "The effect of CNT volume fraction on the magneto-thermo-electro-mechanical behavior of smart nanocomposite cylinder", *J. Mech. Sci. Technol.*, **26**(8), 2565-2572. <https://doi.org/10.1007/s12206-012-0639-5>
- Hajmohammad, M.H., Zarei, M.S., Sepehr, M. and Abtahi, N. (2018), "Bending and buckling analysis of functionally graded annular microplate integrated with piezoelectric layers based on layerwise theory using DQM", *Aerosp. Sci. Technol.*, **79**, 679-688. <https://doi.org/10.1016/j.ast.2018.05.055>
- Huang, Z., Huang, X., Li, W., Mei, L. and Liew J.Y.R. (2019), "Experimental behavior of VHSC encased composite stub column under compression and end moment", *Steel Compos. Struct., Int. J.*, **31**(1), 69-83.  
<https://doi.org/10.12989/scs.2019.31.1.069>
- Karami, B., Shahsavari, D., Janghorban, M. and Tounsi, A. (2019), "Resonance behavior of functionally graded polymer composite nanoplates reinforced with graphene nanoplatelets", *Int. J. Mech. Sci.*, **156**, 94-105.  
<https://doi.org/10.1016/j.ijmecsci.2019.03.036>
- Khan, Q.S., Sheikh, M.N. and Hadi, M.N.S. (2019), "Experimental and analytical investigations of CFFT columns with and without FRP bars under concentric compression", *Steel Compos. Struct., Int. J.*, **30**(6), 591-601.  
<https://doi.org/10.12989/scs.2019.30.6.591>
- Kim, J., Žur, K.K. and Reddy, J.N. (2019), "Bending, free vibration, and buckling of modified couples stress-based functionally graded porous micro-plates", *Compos. Struct.*, **209**, 879-888. <https://doi.org/10.1016/j.compstruct.2018.11.023>
- Lei, Z.X., Liew, K.M. and Yu, J.L. (2013), "Buckling analysis of functionally graded carbon nanotube-reinforced composite plates using the element-free kp-Ritz method", *Compos. Struct.*, **98**, 160-168. <https://doi.org/10.1016/j.compstruct.2012.11.006>
- Li, Q., Wu, D., Chen, X., Liu, L. and Gao, W. (2018), "Nonlinear vibration and dynamic buckling analyses of sandwich functionally graded porous plate with graphene platelet reinforcement resting on Winkler-Pasternak elastic foundation", *Int. J. Mech. Sci.*, **148**, 596-610.  
<https://doi.org/10.1016/j.ijmecsci.2018.09.020>
- Liu, Y., Su, S., Huang, H. and Liang, Y. (2019), "Thermal-mechanical coupling buckling analysis of porous functionally graded sandwich beams based on physical neutral plane", *Compos. Part B: Eng.*, **168**, 236-242.  
<https://doi.org/10.1016/j.compositesb.2018.12.063>
- Mohammadimehr, M. and Alimirzaei, S. (2017), "Buckling and free vibration analysis of tapered FG- CNTRC micro Reddy beam under longitudinal magnetic field using FEM", *Smart Struct. Syst., Int. J.*, **19**(3), 309-322.  
<https://doi.org/10.12989/sss.2017.19.3.309>
- Mohammadimehr, M. and Mehrabi, M. (2017), "Stability and free vibration analyses of double-bonded micro composite sandwich cylindrical shells conveying fluid flow", *Appl. Math. Model.*, **47**, 685-709. <https://doi.org/10.1016/j.apm.2017.03.054>
- Mohammadimehr, M. and Mehrabi, M. (2018), "Electro-thermo-mechanical vibration and stability analyses of double-bonded micro composite sandwich piezoelectric tubes conveying fluid flow", *Appl. Math. Model.*, **60**, 255-272.  
<https://doi.org/10.1016/j.apm.2018.03.008>
- Mohammadimehr, M. and Mostafavifar, M. (2016), "Free vibration analysis of sandwich plate with a transversely flexible core and FG-CNTs reinforced nanocomposite face sheets subjected to magnetic field and temperature-dependent material properties using SGT", *Compos. Part B: Eng.*, **94**, 253-270.  
<https://doi.org/10.1016/j.compositesb.2016.03.030>
- Mohammadimehr, M. and Shahedi, S. (2016), "Nonlinear magneto-electro-mechanical vibration analysis of double-bonded sandwich Timoshenko microbeams based on MSGT using GDQM", *Steel Compos. Struct., Int. J.*, **21**(1), 1-36.  
<https://doi.org/10.12989/scs.2016.21.1.001>
- Mohammadimehr, M. and Shahedi, S. (2017), "High-order buckling and free vibration analysis of two types sandwich beam including AL or PVC-foam flexible core and CNTs reinforced nanocomposite face sheets using GDQM", *Compos. Part B: Eng.*, **108**, 91-107.  
<https://doi.org/10.1016/j.compositesb.2016.09.040>
- Mohammadimehr M., Roustae Navi B., and Ghorbanpour Arani A. (2015), "Free vibration of viscoelastic double-bonded polymeric nanocomposite plates reinforced by FG-SWCNTs using MSGT, sinusoidal shear deformation theory and meshless method", *Compos. Struct.*, **131**, 654-671.  
<https://doi.org/10.1016/j.compstruct.2015.05.077>
- Mohammadimehr, M., Mohandes, M. and Moradi, M. (2016a), "Size dependent effect on the buckling and vibration analysis of double-bonded nanocomposite piezoelectric plate reinforced by boron nitride nanotube based on modified couple stress theory", *J. Vib. Control*, **22**(7), 1790-1807.  
<https://doi.org/10.1177/1077546314544513>
- Mohammadimehr, M., Farahi, M.J. and Alimirzaei, S. (2016b), "Vibration and wave propagation analysis of twisted micro-beam using strain gradient theory", *Appl. Math. Mech.*, **37**(10), 1375-1392. <https://doi.org/10.1007/s10483-016-2138-9>
- Mohammadimehr, M., Mohammadimehr, M.A. and Dashti, P. (2016c), "Size-dependent effect on biaxial and shear nonlinear buckling analysis of nonlocal isotropic and orthotropic microplate based on surface stress and modified couple stress theories using differential quadrature method (DQM)", *Appl. Math. Mech.*, **37**(4), 529-554.  
<https://doi.org/10.1007/s10483-016-2045-9>
- Mohammadimehr, M., Navi, B.R. and Arani, A.G. (2016d), "Modified strain gradient Reddy rectangular plate model for biaxial buckling and bending analysis of double-coupled piezoelectric polymeric nanocomposite reinforced by FG-SWNT", *Compos. Part B: Eng.*, **87**, 132-148.  
<https://doi.org/10.1016/j.compositesb.2015.10.007>
- Mohammadimehr, M., Rostami, R. and Arefi, M. (2016e), "Electro-elastic analysis of a sandwich thick plate considering FG core and composite piezoelectric layers on Pasternak foundation using TSDT", *Steel Compos. Struct., Int. J.*, **20**(3), 513-544. <https://doi.org/10.12989/scs.2016.20.3.513>
- Mohammadimehr, M., Mohammadi-Dehabadi, A.A., Akhavan Alavi, S.M., Alambeigi, K., Bamdad, M., Yazdani, R. and Hanifehlou, S. (2018a), "Bending, buckling, and free vibration analyses of carbon nanotube reinforced composite beams and experimental tensile test to obtain the mechanical properties of

- nanocomposite”, *Steel Compos. Struct., Int. J.*, **29**(3), 405-422. <https://doi.org/10.12989/scs.2018.29.3.405>
- Mohammadimehr, M., Mehrabi, M., Hadizadeh, H. and Hadizadeh, H. (2018b), “Surface and size dependent effects on static, buckling, and vibration of micro composite beam under thermo-magnetic fields based on strain gradient theory”, *Steel Compos. Struct., Int. J.*, **26**(4), 513-531. <https://doi.org/10.12989/scs.2018.26.4.513>
- Mohammadimehr, M., Shabani Nejad, E. and Mehrabi, M. (2018c), “Buckling and vibration analyses of MGSGT double-bonded micro composite sandwich SSDT plates reinforced by CNTs and BNNTs with isotropic foam & flexible transversely orthotropic cores”, *Struct. Eng. Mech., Int. J.*, **65**(4), 491-504. <https://doi.org/10.12989/sem.2018.65.4.491>
- Moradi-Dastjerdi, R. and Aghadavoudi, F. (2018), “Static analysis of functionally graded nanocomposite sandwich plates reinforced by defected CNT”, *Compos. Struct.*, **200**, 839-848. <https://doi.org/10.1016/j.compstruct.2018.05.122>
- Nasihatgozar, M., Daghigh, V., Eskandari, M., Nikbin, K. and Simoneau, A. (2016), “Buckling analysis of piezoelectric cylindrical composite panels reinforced with carbon nanotubes”, *Int. J. Mech. Sci.*, **107**, 69-79. <https://doi.org/10.1016/j.ijmecsci.2016.01.010>
- Saidi, A.R., Bahaadini, R. and Majidi-Mozafari, K. (2019), “On vibration and stability analysis of porous plates reinforced by graphene platelets under aerodynamical loading”, *Compos. Part B: Eng.*, **164**, 778-799. <https://doi.org/10.1016/j.compositesb.2019.01.074>
- Sharif Zarei, M., Hajmohammad, M.H., Mostafavifar, M. and Mohammadimehr, M. (2018), “Influence of temperature change and humidity condition on free vibration analysis of a nano composite sandwich plate resting on orthotropic Pasternak foundation by considering agglomeration effect”, *J. Sandw. Struct. Mater.* <https://doi.org/10.1177/1099636217735118>
- Sobhy, M. and Zenkour, A.M. (2018), “Magnetic field effect on thermomechanical buckling and vibration of viscoelastic sandwich nanobeams with CNT reinforced face sheets on a viscoelastic substrate”, *Compos. Part B: Eng.*, **154**, 492-506. <https://doi.org/10.1016/j.compositesb.2018.09.011>
- Sofiyev, A.H. (2014), “The vibration and buckling of sandwich cylindrical shells covered by different coatings subjected to the hydrostatic pressure”, *Compos. Struct.*, **117**, 124-134. <https://doi.org/10.1016/j.compstruct.2014.06.025>
- Sofiyev, A.H. (2018), “Application of the FOSDT to the solution of buckling problem of FGM sandwich conical shells under hydrostatic pressure”, *Compos. Part B: Eng.*, **144**, 88-98. <https://doi.org/10.1016/j.compositesb.2018.01.025>
- Sofiyev, A.H. (2019), “Review of research on the vibration and buckling of the FGM conical shells”, *Compos. Struct.*, **211**, 301-317. <https://doi.org/10.1016/j.compstruct.2018.12.047>
- Sofiyev, A.H., Hui, D., Valiyev, A.A., Kadioglu, F., Turkaslan, S., Yuan, G.Q., Kalpakci, V. and Özdemir, A. (2016), “Effects of shear stresses and rotary inertia on the stability and vibration of sandwich cylindrical shells with FGM core surrounded by elastic medium”, *Mech. Based Des. Struct. Mach., Int. J.*, **44**(4), 384-404. <https://doi.org/10.1080/15397734.2015.1083870>
- Sofiyev, A.H., Zerini, Z., Allahverdiev, B.P., Hui, D., Turan, F. and Erdem, H. (2017), “The dynamic instability of FG orthotropic conical shells within the SDT”, *Steel Compos. Struct., Int. J.*, **25**(5), 581-591. <https://doi.org/10.12989/scs.2017.25.5.581>
- Timoshenko, S. and Gere, J. (1961), *Theory of elastic stability*, (2nd Edition), Mc Graw Hill, New York, NY, USA.
- Ventsel, E. and Krauthammer, T. (2001), *Thin plates and shells: theory: analysis, and applications*, The Pennsylvania State University; University Park, PA, USA, 0-8247-0575-0.
- Vinson, J.R. (2005), *Sandwich Structures: Past, Present, and Future. Sandwich Structures. 7: Advancing with Sandwich Structures and Materials*, Berlin/Heidelberg: Springer-Verlag, 3-12.
- Xie, Q., Sinaei, H., Shariati, M., Mohamad, E.T. and Bui, D.T. (2019), “An experimental study on the effect of CFRP on behavior of reinforced concrete beam column connections”, *Steel Compos. Struct., Int. J.*, **30**(5), 433-441. <https://doi.org/10.12989/scs.2019.30.5.433>
- Yang, Z. and He, D. (2017), “Vibration and buckling of orthotropic functionally graded micro-plates on the basis of a re-modified couple stress theory”, *Results in Phys.*, **7**, 3778-3787. <https://doi.org/10.1016/j.rinp.2017.09.026>
- Zhang, L.W., Song, G. and Liew, K.M. (2015), “Nonlinear bending analysis of FG-CNT reinforced composite thick plates resting on Pasternak foundations using the element-free IMLS-Ritz method”, *Compos. Struct.*, **128**, 165-175. <https://doi.org/10.1016/j.compstruct.2015.03.011>
- Zhang, Z.J., Zhang, Q.C., Li, F.C., Yang, J.W., Liu, J.W., Liu, Z.Y. and Jin, F. (2019), “Modal characteristics of micro-perforated sandwich beams with square honeycomb-corrugation hybrid cores: A mixed experimental-numerical study”, *Thin-Wall. Struct.*, **137**, 185-196. <https://doi.org/10.1016/j.tws.2019.01.004>

CC

## Appendix A

$\eta_{ijk}$ ,  $\chi_{ij}$  and  $\gamma_i$  are deviatoric stretch gradient tensor, symmetric rotation gradient tensor and dilatation gradient vector, respectively, and  $D_i$  and  $E_i$  denote the electric displacement and the electric field, respectively, that they can be obtained as the following form

$$\varepsilon_{ij} = \frac{1}{2} \left( \frac{\partial u_i(x, z, t)}{\partial x_j} + \frac{\partial u_j(x, z, t)}{\partial x_i} \right) \quad (\text{A1})$$

$$\gamma_i = \frac{\partial \varepsilon_{kk}}{\partial x_i} \quad (\text{A2})$$

$$\chi_{ij}^{(s)} = \frac{1}{2} \left( e_{ipq} \frac{\partial \varepsilon_{qj}}{\partial x_p} + e_{jpa} \frac{\partial \varepsilon_{qi}}{\partial x_p} \right) \quad (\text{A3})$$

$$\begin{aligned} \eta_{ijk}^{(1)} = & \frac{1}{3} (\varepsilon_{jki} + \varepsilon_{kij} + \varepsilon_{ijk}) \\ & - \frac{1}{15} \delta_{ij} (\varepsilon_{mm,k} + 2\varepsilon_{mj,m}) \\ & - \frac{1}{15} \delta_{jk} (\varepsilon_{mm,i} + 2\varepsilon_{mi,m}) \\ & - \frac{1}{15} \delta_{ki} (\varepsilon_{mm,j} + 2\varepsilon_{mj,m}) \end{aligned} \quad (\text{A4})$$

$$\sigma_{ij} = Q_{ij} \varepsilon_{ij} - e^T E_i \quad (\text{A5})$$

$$P_i = 2Gl_0^2 \gamma_i \quad (\text{A6})$$

$$\tau_{ijk}^{(1)} = 2Gl_1^2 \eta_{ijk}^{(1)} \quad (\text{A7})$$

$$m_{ij}^{(s)} = 2Gl_2^2 \chi_{ij}^{(s)} \quad (\text{A8})$$

In the above relations,  $u_i$  represents the displacement field components,  $G$  the shear modulus,  $\delta$  the Kronecker delta, and  $e_{ijk}$  permutation symbol, which, in accordance with Eq. (A9), can take values of zero, 1, and -1. Also  $l_0$ ,  $l_1$  and  $l_2$  known as three material length scale parameters are the length of a substance, whose values are according to Table 1 for classical, modified couple stress and modified strain gradient theories.

$$\begin{cases} e_{123} = e_{231} = e_{312} = 1 \\ e_{321} = e_{132} = e_{213} = -1 \end{cases} \quad (\text{A9})$$

## Appendix B

The values for higher order stresses and electrical displacement are defined as relationships (B1) to (B24).

$$M_{xx} = \int_{\frac{hc}{2}}^{\frac{H}{2}} \sigma_{xx} z dz + \int_{-\frac{hc}{2}}^{\frac{hc}{2}} \sigma_{xx} z dz + \int_{-\frac{H}{2}}^{-\frac{hc}{2}} \sigma_{xx} z dz \quad (\text{B1})$$

$$M_{yy} = \int_{\frac{hc}{2}}^{\frac{H}{2}} \sigma_{yy} z dz + \int_{-\frac{hc}{2}}^{\frac{hc}{2}} \sigma_{yy} z dz + \int_{-\frac{H}{2}}^{-\frac{hc}{2}} \sigma_{yy} z dz \quad (\text{B2})$$

$$M_{xy} = \int_{\frac{hc}{2}}^{\frac{H}{2}} \tau_{xy} z dz + \int_{-\frac{hc}{2}}^{\frac{hc}{2}} \tau_{xy} z dz + \int_{-\frac{H}{2}}^{-\frac{hc}{2}} \tau_{xy} z dz \quad (\text{B3})$$

$$\begin{aligned} P_{1x} = & \int_{\frac{hc}{2}}^{\frac{H}{2}} 2Gl_0^2 \gamma_x z dz + \int_{-\frac{hc}{2}}^{\frac{hc}{2}} 2Gl_0^2 \gamma_x z dz \\ & + \int_{-\frac{H}{2}}^{-\frac{hc}{2}} 2Gl_0^2 \gamma_x z dz \end{aligned} \quad (\text{B4})$$

$$\begin{aligned} P_{1y} = & \int_{\frac{hc}{2}}^{\frac{H}{2}} 2Gl_0^2 \gamma_y z dz + \int_{-\frac{hc}{2}}^{\frac{hc}{2}} 2Gl_0^2 \gamma_y z dz \\ & + \int_{-\frac{H}{2}}^{-\frac{hc}{2}} 2Gl_0^2 \gamma_y z dz \end{aligned} \quad (\text{B5})$$

$$\begin{aligned} P_{0z} = & \int_{\frac{hc}{2}}^{\frac{H}{2}} 2Gl_0^2 \gamma_y dz + \int_{-\frac{hc}{2}}^{\frac{hc}{2}} 2Gl_0^2 \gamma_y dz \\ & + \int_{-\frac{H}{2}}^{-\frac{hc}{2}} 2Gl_0^2 \gamma_y dz \end{aligned} \quad (\text{B6})$$

$$\begin{aligned} T_{1xxx} = & \int_{\frac{hc}{2}}^{\frac{H}{2}} 2Gl_1^2 \eta_{xxx} z dz + \int_{-\frac{hc}{2}}^{\frac{hc}{2}} 2Gl_1^2 \eta_{xxx} z dz \\ & + \int_{-\frac{H}{2}}^{-\frac{hc}{2}} 2Gl_1^2 \eta_{xxx} z dz \end{aligned} \quad (\text{B7})$$

$$\begin{aligned} T_{1xxy} = & \int_{\frac{hc}{2}}^{\frac{H}{2}} 2Gl_1^2 \eta_{xxy} z dz + \int_{-\frac{hc}{2}}^{\frac{hc}{2}} 2Gl_1^2 \eta_{xxy} z dz \\ & + \int_{-\frac{H}{2}}^{-\frac{hc}{2}} 2Gl_1^2 \eta_{xxy} z dz \end{aligned} \quad (\text{B8})$$

$$\begin{aligned} T_{0xxz} = & \int_{\frac{hc}{2}}^{\frac{H}{2}} 2Gl_1^2 \eta_{xxz} dz + \int_{-\frac{hc}{2}}^{\frac{hc}{2}} 2Gl_1^2 \eta_{xxz} dz \\ & + \int_{-\frac{H}{2}}^{-\frac{hc}{2}} 2Gl_1^2 \eta_{xxz} dz \end{aligned} \quad (\text{B9})$$

$$T_{0xyz} = \int_{\frac{hc}{2}}^{\frac{H}{2}} 2Gl_1^2 \eta_{xyz} dz + \int_{-\frac{hc}{2}}^{\frac{hc}{2}} 2Gl_1^2 \eta_{xyz} dz + \int_{-\frac{H}{2}}^{-\frac{hc}{2}} 2Gl_1^2 \eta_{xyz} dz \quad (\text{B10})$$

$$T_{1xyy} = \int_{\frac{hc}{2}}^{\frac{H}{2}} 2Gl_1^2 \eta_{xyy} z dz + \int_{-\frac{hc}{2}}^{\frac{hc}{2}} 2Gl_1^2 \eta_{xyy} z dz + \int_{-\frac{H}{2}}^{-\frac{hc}{2}} 2Gl_1^2 \eta_{xyy} z dz \quad (\text{B11})$$

$$T_{1xzz} = \int_{\frac{hc}{2}}^{\frac{H}{2}} 2Gl_1^2 \eta_{xzz} z dz + \int_{-\frac{hc}{2}}^{\frac{hc}{2}} 2Gl_1^2 \eta_{xzz} z dz + \int_{-\frac{H}{2}}^{-\frac{hc}{2}} 2Gl_1^2 \eta_{xzz} z dz \quad (\text{B12})$$

$$T_{1yyy} = \int_{\frac{hc}{2}}^{\frac{H}{2}} 2Gl_1^2 \eta_{yyy} z dz + \int_{-\frac{hc}{2}}^{\frac{hc}{2}} 2Gl_1^2 \eta_{yyy} z dz + \int_{-\frac{H}{2}}^{-\frac{hc}{2}} 2Gl_1^2 \eta_{yyy} z dz \quad (\text{B13})$$

$$T_{0yyz} = \int_{\frac{hc}{2}}^{\frac{H}{2}} 2Gl_1^2 \eta_{yyz} dz + \int_{-\frac{hc}{2}}^{\frac{hc}{2}} 2Gl_1^2 \eta_{yyz} dz + \int_{-\frac{H}{2}}^{-\frac{hc}{2}} 2Gl_1^2 \eta_{yyz} dz \quad (\text{B14})$$

$$T_{1yzz} = \int_{\frac{hc}{2}}^{\frac{H}{2}} 2Gl_1^2 \eta_{yzz} z dz + \int_{-\frac{hc}{2}}^{\frac{hc}{2}} 2Gl_1^2 \eta_{yzz} z dz + \int_{-\frac{H}{2}}^{-\frac{hc}{2}} 2Gl_1^2 \eta_{yzz} z dz \quad (\text{B15})$$

$$T_{0zzz} = \int_{\frac{hc}{2}}^{\frac{H}{2}} 2Gl_1^2 \eta_{zzz} dz + \int_{-\frac{hc}{2}}^{\frac{hc}{2}} 2Gl_1^2 \eta_{zzz} dz + \int_{-\frac{H}{2}}^{-\frac{hc}{2}} 2Gl_1^2 \eta_{zzz} dz \quad (\text{B16})$$

$$R_{0x} = \int_{\frac{hc}{2}}^{\frac{H}{2}} 2Gl_2^2 \chi_{xx} dz + \int_{-\frac{hc}{2}}^{\frac{hc}{2}} 2Gl_2^2 \chi_{xx} dz + \int_{-\frac{H}{2}}^{-\frac{hc}{2}} 2Gl_2^2 \chi_{xx} dz \quad (\text{B17})$$

$$R_{0y} = \int_{\frac{hc}{2}}^{\frac{H}{2}} 2Gl_2^2 \chi_{yy} dz + \int_{-\frac{hc}{2}}^{\frac{hc}{2}} 2Gl_2^2 \chi_{yy} dz + \int_{-\frac{H}{2}}^{-\frac{hc}{2}} 2Gl_2^2 \chi_{yy} dz \quad (\text{B18})$$

$$R_{0yx} = \int_{\frac{hc}{2}}^{\frac{H}{2}} 2Gl_2^2 \chi_{xy} dz + \int_{-\frac{hc}{2}}^{\frac{hc}{2}} 2Gl_2^2 \chi_{xy} dz + \int_{-\frac{H}{2}}^{-\frac{hc}{2}} 2Gl_2^2 \chi_{xy} dz \quad (\text{B19})$$

$$D_{1x} = \int_{\frac{hc}{2}}^{\frac{H}{2}} \left( -e_{11z} \frac{\partial^2}{\partial x^2} w(x, y, t) - e_{12z} \frac{\partial^2}{\partial y^2} w(x, y, t) \right) \cos^2 \left( \frac{\pi z}{h} \right) dz + \int_{-\frac{H}{2}}^{-\frac{hc}{2}} \left( \frac{\partial}{\partial x} \psi(x, y, t) \cos \left( \frac{\pi z}{h} \right) \eta_{11} - e_{11z} \frac{\partial^2}{\partial x^2} w(x, y, t) - e_{12z} \frac{\partial^2}{\partial y^2} w(x, y, t) \right) \cos^2 \left( \frac{\pi z}{h} \right) dz \quad (\text{B20})$$

$$D_{1y} = \int_{\frac{hc}{2}}^{\frac{H}{2}} \left( \eta_{22} \frac{\partial}{\partial y} \psi(x, y, t) \right) \left( \frac{\pi z}{h} \right) dz + \int_{-\frac{H}{2}}^{-\frac{hc}{2}} \left( \eta_{22} \frac{\partial}{\partial y} \psi(x, y, t) \right) \cos^2 \left( \frac{\pi z}{h} \right) dz \quad (\text{B21})$$

$$D_{1z} = \int_{\frac{hc}{2}}^{\frac{H}{2}} -h^2 \eta_{33} \psi(x, y, t) \sin^2 \left( \frac{\pi z}{h} \right) \pi^2 dz + \int_{-\frac{H}{2}}^{-\frac{hc}{2}} -h^2 \eta_{33} \psi(x, y, t) \sin^2 \left( \frac{\pi z}{h} \right) \pi^2 dz \quad (\text{B22})$$

$$N_{0xz} = \int_{\frac{hc}{2}}^{\frac{H}{2}} \sigma_{xz}^t dz + \int_{-\frac{hc}{2}}^{\frac{hc}{2}} \sigma_{xz}^c dz + \int_{-\frac{H}{2}}^{-\frac{hc}{2}} \sigma_{xz}^b dz \quad (\text{B23})$$

$$N_{0zy} = \int_{\frac{hc}{2}}^{\frac{H}{2}} \sigma_{yz}^t dz + \int_{-\frac{hc}{2}}^{\frac{hc}{2}} \sigma_{yz}^c dz + \int_{-\frac{H}{2}}^{-\frac{hc}{2}} \sigma_{yz}^b dz \quad (\text{B24})$$